Morphology of Polyurethanes at Various Length Scale: The Influence of Chain Structure

Abhinay Mishra, Pralay Maiti

School of Materials Science and Technology, Institute of Technology, Banaras Hindu University, Varanasi 221005, India.

Received 30 July 2010; accepted 3 October 2010
DOI 10.1002/app.33525
Published online 14 February 2011 in Wiley Online Library (wileyonlinelibrary.com).

ABSTRACT: Micro-structural investigation of polyurethanes (PUs) with different chain structure has been reported. Polarized optical microscopic studies of aliphatic polyurethanes demonstrate the development of micro clusters with increasing hard segment content (HSC) and crystallization. DSC and XRD results support the crystalline and amorphous nature of aliphatic and aromatic PUs, respectively. Self-assembled biphasic morphology is discernible in aliphatic polyurethane while nanometer size domains are observed in aromatic PUs. The dimension of micro-domain has been measured by using AFM and established its size as independent of hard segment content. The self-assembly is greater for higher HSC aliphatic PUs leading to the formation of bigger domain while the meager hydrogen bond formation restricts the domain size of aromatic polyurethanes. Segmented morphology of surface as well as in bulk of aliphatic polyurethanes is evident from SEM and TEM images and grows with increasing HSC. In contrast, homogeneous and amorphous nature has been observed for aromatic PUs. In situ segregation of phases in aliphatic PUs have been captured through light transmittance and optical images which is categorically absent in aromatic polyurethane. © 2011 Wiley Periodicals, Inc. J Appl Polym Sci 120: 3546–3555, 2011

Key words: polyurethane; morphology; self-assembly; structure

INTRODUCTION

Segmented polyurethanes are intriguing class of thermoplastic elastomers[1–4] which was initially developed as a replacement for rubber but now it is utilized in the production of high-performance elastomeric product. It has potential use in biomedical tissue engineering,[5,6] molecular recognition,[7] biocompatible materials, durable coating,[8] and shape memory materials.[9–12] Structure property correlation is the prime prospective arises due to thermodynamic incompatibility between the hard and soft segments. It drives the polymer into two phase morphology in which crystalline hard micro domains are hydrogen-bonded to form larger domains. These hard microdomains form fibrillar, globular, cylindrical, or lamellar structures within a continuous soft matrix and reinforces the soft matrix by acting as physical crosslinking sites depending on the specific segmental composition.[13–22] In addition, the intersegmental hydrogen-bonding capability of the hard segment increases the cohesiveness of the hard domains and association of the hard domains provides additional driving force for phase separation.[23–27]

Polyurethane is fascinating system to tune its properties and structural variation with its self-assembling morphology.[28–38] McLean et al.[35] has reported nanophase separated hard segment domains in solvent cast films of segmented polyurethane and a segmented micrographs of polyamide elastomer have been taken in real space using phase and topographical information from tapping-mode AFM techniques. Domain size, distribution, shape, orientation, spacing, and uniformity in space have been extracted from AFM images. Further, Sheth et al.[36] has reported hard segment phase connectivity and percolation model for segmented poly(urethane urea) copolymers. The major outcome of their studies was the tapping-mode AFM phase image of the poly(urethane urea) sample without hard segment branching which exhibited in the form of long ribbon like hard domains percolated in the soft matrix. Later, they have also reported time-dependent development of hard phase from short rods to well defined percolated structure through AFM phase studies of segmented polyurethane with monodisperse hard segments based on 1, 4-phenylene diisocyanate.[37] Recently we have reported step by step self-assembly of aliphatic polyurethanes

Correspondence to: P. Maiti (pmaiti.mst@itbhu.ac.in).
Contract grant sponsor: Council of Scientific and Industrial Research (CSIR), New Delhi.
Contract grant sponsor: Council of Scientific and Industrial Research (CSIR); contract grant number: 22(0399)/06/EMR-II.

TABLE I
Characteristics of Polyurethane Samples and Their Designation

% HSC	Diisocyanate	Molar Ratios of PTMG : Diisocyanate : BD	Designation
10	HMDI	1 : 1.6 : 0.6	PU10
50	HMDI	1 : 11.2 : 10.2	PU50
80	HMDI	1 : 45 : 44	PU80
70	MDI	1 : 21 : 20	MDI70
70	TDI	1 : 26 : 25	TDI70

from nanometer to micrometer length scale and its effect on the mechanical properties.[38] Further preceding the studies on aliphatic polyurethanes we have focused our attention towards the development of morphology and its correlation to the microstructure.

In this study, comparison of morphological development has been made for different chain structure of polyurethanes. The correlation of microstructure and phase segregated morphology of aliphatic polyurethanes in contrast to aromatic polyurethanes has been described. Microstructures have been studied in a range of length scale of micron to nanometer with the help of POM, AFM, SEM, and XRD showing the structure-property relationship of supramolecular polyurethanes. The self-assembly pattern of the hard segment zone starting from nanometer level to micron size have been discussed. Separation of phases has also been described through light transmittance of polyurethanes with different chain structure.

EXPERIMENTAL

Materials and synthesis

Poly tetra methylene glycol (PTMG) (Terathane, Sigma Aldrich) with number average molecular weight (M_n) 2900 g/mol, 4,4′-methylene bis(phenyl isocyanate) (MDI) (Sigma Aldrich) and 2,4-tolylene diisocyanate (TDI) (Sigma Aldrich) 1,6-hexa methylene diisocyanate (HMDI) (Merck Germany) and 1,4-butanediol (BD) (Merck Germany) were used as received. The catalyst dibutyltin dilaurate was supplied by Himedia and spectroscopic grade dimethyl formamide (DMF) was provided by Loba Chemie.

Polyurethanes (PU) were synthesized by condensation polymerization process. Prepolymer formation is commonly referred as first step in which polyol and excess diisocyanate produces an isocyanate-terminated molecule (prepolymer). The prepolymers were usually low molecular weight viscous liquid or low melting solid. In the second step, prepolymers were reacted with a chain extender (usually either aliphatic or aromatic diols) to produce the segmented polyurethanes. By varying the diol/chain extender and diisocyanate content, we produced different hard segment content (HSC) PU starting from 10 to 80% using the above method. In the first stage, polyol (PTMG), and diisocyanate (HMDI/TDI/MDI) was mixed at a constant temperature of 70°C for 4 h to form an isocyanate-terminated prepolymer. In the second stage, the prepolymer was treated with 1,4-butanediol (BD) as a chain extender in presence of catalyst (dibutyltin dilaurate) and little amount of solvent (DMF) to avoid solidification with rapid stirring at the same temperature for 24 h in an inert atmosphere. The polymer was extracted by pouring the solution in deionized water and dried in vacuum at 0.1 Torr and 60°C for 48 h. Thus, polyurethanes of different hard segment contents were synthesized using different molar ratios of PTMG, Diisocyanate (aliphatic HMDI and aromatic TDI and MDI) and BD as indicated in Table I. The designation and details of polyurethanes are also shown in Table I. Henceforth, HMDI based polyurethanes will be termed as aliphatic and TDI- and MDI-based PUs as aromatic polyurethanes. The numbers after PU indicate the hard segment content in percentage. The molecular weight of the aliphatic polyurethane is $\sim$ 35,000 for all the HSC as measured by using GPC while the molecular weight of MDI-based PU was $\sim$ 80,000.

CHARACTERIZATION

X-ray diffraction

X-ray diffraction was performed using Bruker AXS D8 Advance wide-angle X-ray diffractometer with a graphite monochromator using CuKα source with a wavelength of 0.154 nm. The generator was operated at 40 kV and 20 mA. The thin sheet of the samples were placed on a quartz sample holder at room temperature and were scanned at diffraction angle 2θ from 1° to 40° at the scanning rate of 1° min^{-1}.

Differential scanning calorimetry

The melting, crystallization temperatures and heats of fusion of PUs were determined via DSC using Mettler 832 over a temperature range of −20 to 250°C. The samples were heated at the scan rate of 10°C/min. The peak temperature and enthalpy of fusion were measured from the endotherms using a computer attached with the instrument. After the first melting, the samples were cooled down at a constant

rate of 10°C/min to find the crystallization temperature and heat of crystallization in a similar fashion. The DSC was calibrated with indium before use.

Light microscopy

Phase separation behavior of PUs was determined via Mettler hot stage equipped with light source and photodetector. Thin film (~30 μm) of polymer has been placed in a hot stage and the sample was scanned at a heating rate of 3°/min. The transmitted light was detected by photo detector attached with computer. Hot stage was placed on a polarizing optical microscope and the optical images were captured at different temperatures.

Morphological investigation

The morphology of PU was investigated by using scanning electron microscope (SEM), atomic force microscope (AFM) and polarizing optical microscope (POM) while the crystallite size was observed by using transmission electron microscope (TEM).

Scanning electron microscopy

The surface morphology of pure polyurethane flakes was examined with a Hitachi H-7100 scanning electron microscope operated at an accelerating voltage of 10 kV. All the samples were gold-coated by means of a sputtering apparatus under vacuum before observation.

Atomic force microscopy

A NT-MDT multimode atomic force microscope, Russia, controlled by Solver scanning probe was used for surface morphology study. Tapping mode was used with the tip mounted on 100 μm long single beam cantilever with resonant frequency in the rage of 240–255 kHz, and corresponding spring constant of 11.5 N/m. Thin film of ~40 μm was used for AFM studies after suitably processing them through melt pressing. AFM studies of the thin films depend on the free amplitude (A_o) used in this study was between 15 and 30 nm. Most samples were characterized using a set-point amplitude ratio (r_{sp}) between 0.7 and 0.5. r_{sp} is defined as the ratio of the cantilever's oscillating amplitude (in contact) to its freely oscillating amplitude (out of contact). Set-point amplitudes near 1.0 correspond to very light normal forces (soft tapping), and lower r_{sp} corresponds to higher tapping force.

Polarizing optical microscopy

The morphology of thin film (~30 μm) in optical range was examined using a polarizing optical microscope (POM) (Nikon) after quenching the samples at room temperature as well as crystallizing the samples of PU10, PU50, and PU80 at 95°C, 120°C, 145°C, respectively, for 2, 6, 12 h on a Mettler hot stage. The temperature was chosen according to their respective melting points to keep the undercooling same (30° less than the observed melting point). Aromatic PUs were not crystallized because of their amorphous nature.

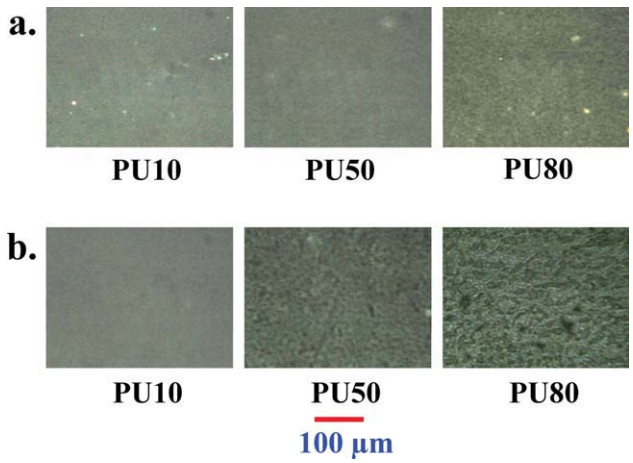

Figure 1 Polarizing optical images of aliphatic PUs showing gradual increase of cluster size with HSC, a) quenched samples and b) crystallized at 95°, 120° and 145°C for PU10, PU50 and PU80, respectively. [Color figure can be viewed in the online issue, which is available at wileyonlinelibrary.com.]

Transmission electron microscopy

The crystallite domain size of the polyurethane was resolved by using TEM (Technai G^2) operated at an accelerating voltage of 100 kV. A thin layer, around 70 nm thick, from the polyurethane sample was sectioned at −80.0°C using a Leica ultra-microtome equipped with a sharp glass knife and afterwards it was stained by using phosphotungstic acid (PTA).

RESULTS AND DISCUSSION

Microstructure through POM

Polarizing optical micrographs of quenched and crystallized aliphatic polyurethanes with the increasing hard segment content have been shown in Figure 1. Two phase morphology is apparent with increasing hard segment content (HSC) of quenched polyurethanes [Fig. 1(a)]. Two phase morphology is evident in the crystallized sample especially for high HSC PU [Fig. 1(b)]. Thin film of PU10, PU50, and PU80 were crystallized at T_c = 95°C, 120°C, 145°C, respectively. The T_cs were chosen below 30°C of the melting point of the respective polymers. Low hard segment PU exhibits homogeneous morphology with

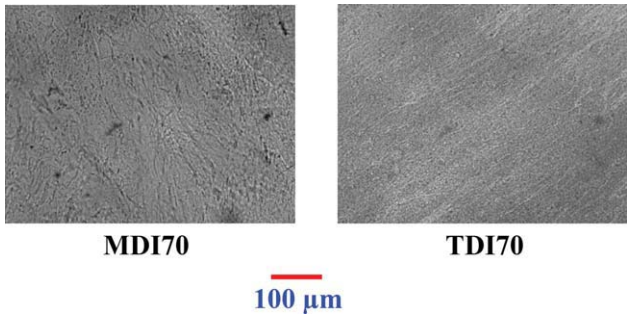

Figure 2 Polarizing optical images of indicated aromatic PUs. [Color figure can be viewed in the online issue, which is available at wileyonlinelibrary.com.]

least segmentization but two phase morphology is clear for higher HSC PU due to enhanced crystallization of greater hard segments. Phase segregation is prominent in crystallized samples in comparison to quenched samples because of enhanced ordering of hard segments at higher temperature. Self-assembled patterns in the form of micro clusters are noticed with increasing hard segment content due to significant hydrogen bonding between hard segment domains which are the crystallizable part in the polymer chains. As a result, crystallinity increases and domain structure becomes prominent with increasing hard segment. Figure 2 shows the optical images of MDI and TDI based aromatic polyurethanes of high HSC. The micro-clusters are not developed as compared with aliphatic PU50 and PU80 which indicate that aromatic polyurethanes are not fairly segmented in contrast to aliphatic polyurethanes. However, two phase morphology/segmentization has occurred in aliphatic PUs and has not been prominent in aromatic polyurethanes.

Crystallinity

DSC thermogrammes of polyurethanes of aliphatic and aromatic origin of higher HSC content have been shown in Figure 3. The melting point is evident in aliphatic PU while high temperature melting behavior has not been observed for aromatic PU, indicating predominantly amorphous nature of aromatic PUs when compared with similar HSC. The low temperature endotherm at ~25°C is related to melting of PTMG in the polymer chain, as confirmed from the melting behavior of pure polyol. Figure 4 shows the melting point (T_m) and the heat of fusion (ΔH) of aliphatic PUs as a function of HSC. Both T_m and ΔH increase with increasing HSC. Hence, high hard segment content PUs exhibit greater crystallinity and, as a result, two phase morphology appear in aliphatic PUs at higher HSC. In contrast, mostly amorphous aromatic TDI- and MDI-based PUs do not exhibit major phase separation but tiny

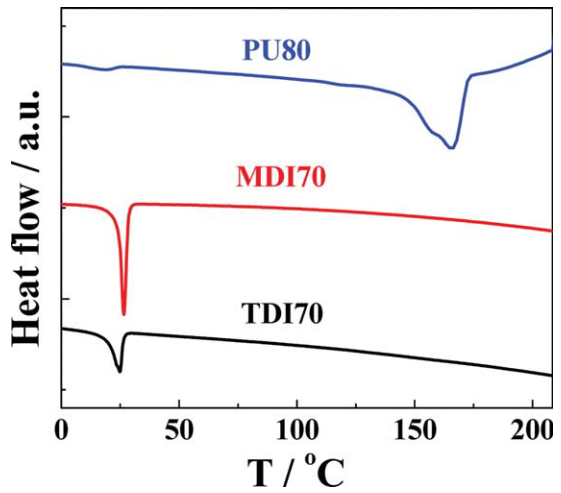

Figure 3 DSC thermograms (exo-up) of indicated PUs (aliphatic and aromatic) in the second run. [Color figure can be viewed in the online issue, which is available at wileyonlinelibrary.com.]

strips appear (Fig. 2) because of small amount of crystallinity arises from polyol part (T_m ~25°C peak). The crystallinity has also been shown in XRD patterns of the aliphatic and aromatic PUs (Fig. 5). Both TDI- and MDI-based aromatic PUs exhibit amorphous halo while distinct crystalline peak is observed for aliphatic PU. It is worthy to mention that lower HSC aliphatic PUs (20–30% HSC) show less crystallinity from XRD and DSC studies for as prepared samples but exhibit mostly amorphous in the second run. During cooling PU50 and PU80 show the crystallization peak at 135°C and 141°C, respectively, but no peak appears for PU10. PTMG belongs to soft segment in PU and the crystalline regions are disorder. In addition, the total crystallinity as

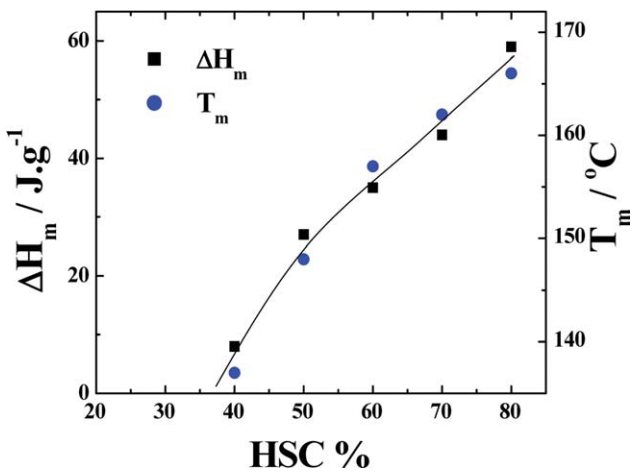

Figure 4 Heat of fusion (ΔH) and melting temperature (T_m) as obtained from DSC of aliphatic PUs as a function of hard segment content. [Color figure can be viewed in the online issue, which is available at wileyonlinelibrary.com.]

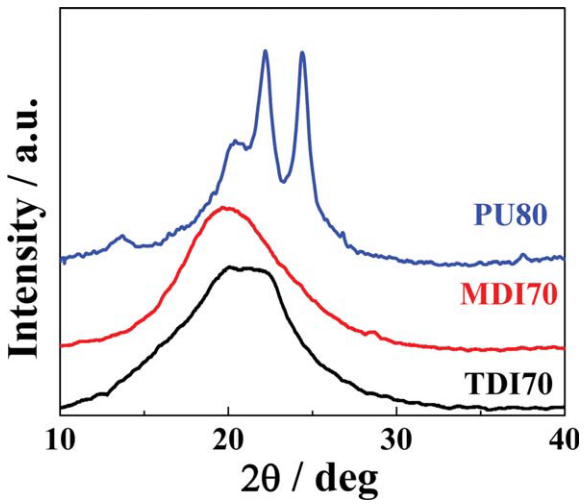

Figure 5 Wide-angle X-ray diffraction patterns of indicated aliphatic and aromatic PUs of high HSC content. The Y-axes have been shifted for the sake of clarity. The numbers after PU indicate the hard segment content in percentage. [Color figure can be viewed in the online issue, which is available at wileyonlinelibrary.com.]

measured from DSC melting endotherm is less ~17 J gm^{-1} for MDI70 against the value of ~60 J gm^{-1} for aliphatic PU80. So, the less crystallinity is not reflected in XRD pattern as separate peak, but presumably it is merged with the broad amorphous hallow. In case of TDI70, two separate peaks is somewhat observed.

Microstructure through AFM

Band patterns have been observed for aliphatic polyurethanes in tapping mode AFM at different hard segment content (Fig. 6). Polymer samples were melt-processed on glass slide. PU10 exhibits ordered hard and soft segmented cylindrical domains, more prominent in the 3D image [Fig. 6(b)]. Well-defined segmented patterns have also been observed for higher HSC PUs and interestingly, the dimension of the individual domain becomes shorter with increasing HSC. The 3D images of aliphatic polyurethanes indicate the relative height profile of the hydrogen bonded crystalline segmented domains. The domain heights gradually increases with increasing hard segment content and are 11, 24, and 42 nm for PU10, PU50, and PU80, respectively. The alternating trough and crest patterns of domains arise from the self-assembled hydrogen bonded hard segments and orient in a periodic arrangement during processing of the film. The alternate dark trough and bright crest patterns describe the amorphous and self-assembled patterns of crystalline domains of polyurethanes in a regular fashion in PU10. The irregular shape of the domains is quite discernible in case of PU50 and PU80. The crystallite zones are gradually increasing and developing in the form of stacked lamellar zones through strong hydrogen bonded interactions in higher HSC PUs. Relatively stronger hydrogen bonded interchain interactions between C═O and N─H groups are responsible for the gradual change of morphology to shorter dimension for high HSC PUs. AFM topographs of aromatic polyurethanes of 70% hard segment content have been shown in Figure 7. Few scattered patches are observed in MDI- and TDI-based aromatic polyurethanes but self-assembled patterns are imperceptible in these higher HSC aromatic polyurethanes. Figure 7(b) shows 3D topographs of aromatic polyurethanes with

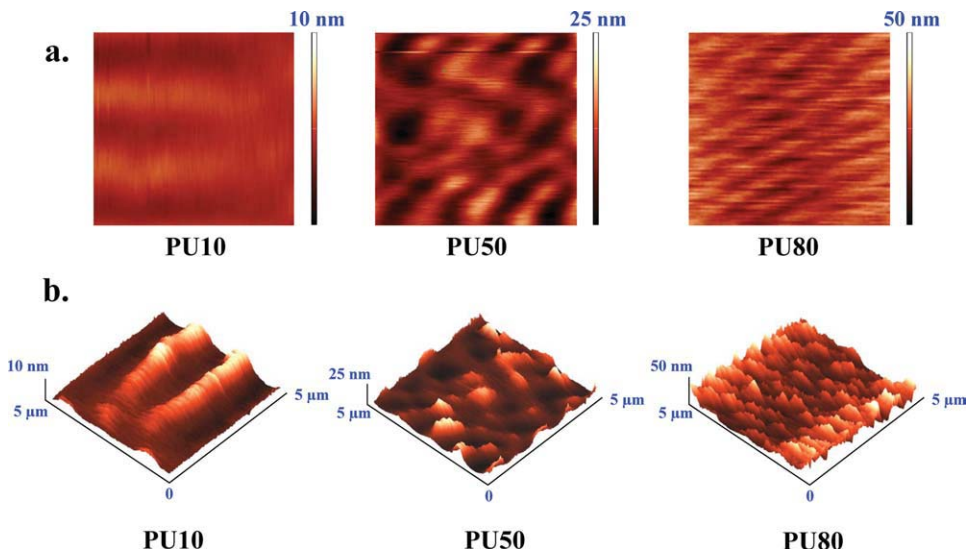

Figure 6 AFM micrographs for various aliphatic PUs which exhibit particular pattern with change in HSC, (a) two dimensional, and (b) three dimensional image. [Color figure can be viewed in the online issue, which is available at wileyonlinelibrary.com.]

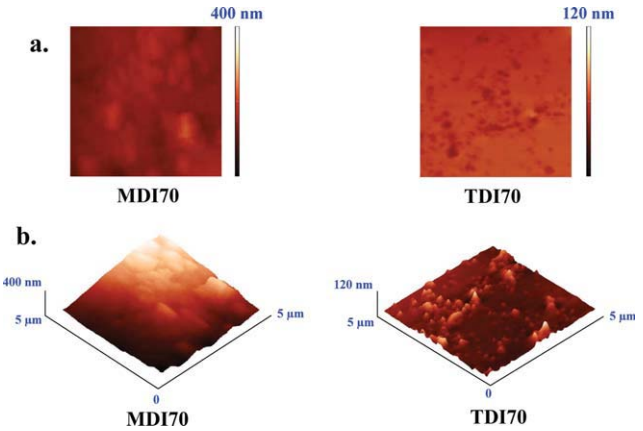

Figure 7 AFM micrographs for various aromatic PUs showing smaller domains for higher HSC, (a) two dimensional, and (b) three dimensional image. [Color figure can be viewed in the online issue, which is available at wileyonlinelibrary.com.]

minimal domains. However, self-assembled features have not been observed in aromatic polyurethanes. Smaller domain in the nanometer scale has also been reported in the literature for aromatic polyurethane[34–36] but no further self-assembly has been reported. We observed the same phenomena for aromatic PUs while aliphatic polyurethanes exhibit extensive self-assembly in addition to structure formation in the nanometer level.

To understand the relative intensity and size of the domain structure, height profiles of the topographs have been presented in Figure 8. It shows the height variation of polyurethane domains scanned across length as shown by the dashed line. Surface morphological height profile histogram was achieved by the interaction of silicon nitride tip with the polyurethane surface. The height profile histogram of PU10 shows two consecutive broadened peaks of ~11 nm height within the range of 5 μm cross-sectional scanned length while four peaks of 24 nm and 10 peaks of 42 nm heights are obtained for PU50 and PU80, respectively, in the same cross-sectional length. The peak width decreases while the peak intensity increases with increasing HSC revealing the formation of smaller and dense domains due to clustering of more number of hard segments for higher HSC PUs. Figure 9 shows the height variation of aromatic polyurethanes as a function of scanned cross-sectional length. The height profile histogram of MDI70 shows two consecutive broadened peaks while two broad peaks of 20 and 120 nm heights are observed for TDI70 in the range of 5 μm cross-sectional length as shown in the left side of the Figure 9. Figures 8 and 9 show the height and width profile for domain structure of aliphatic and aromatic polyurethanes. Individual domain width gradually decreases with increasing HSC and it disappears in

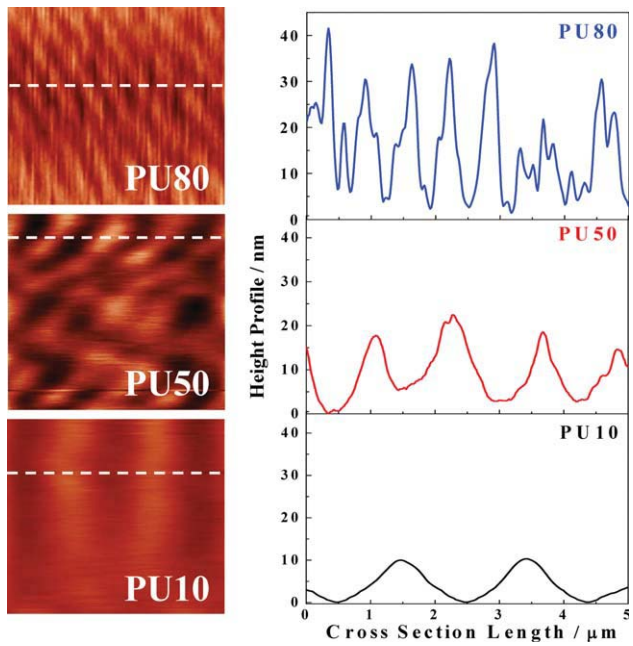

Figure 8 The height profile of the indicated aliphatic PUs (right side figures). The profiles were obtained from the AFM topographs of the portion shown by dashed line in the left side of the figure.

aromatic PUs. If one concentrate on single domain which after scanning further gives rises to 6 to 3 smaller domains (micro-domains) depending upon the HSC content of PUs (Fig. 10). It can be concluded that few micro-domains assembled together to shape a bigger domain as observed in AFM micrographs. For individual domain, the number of micro-domain gradually decreases with increasing HSC. At the

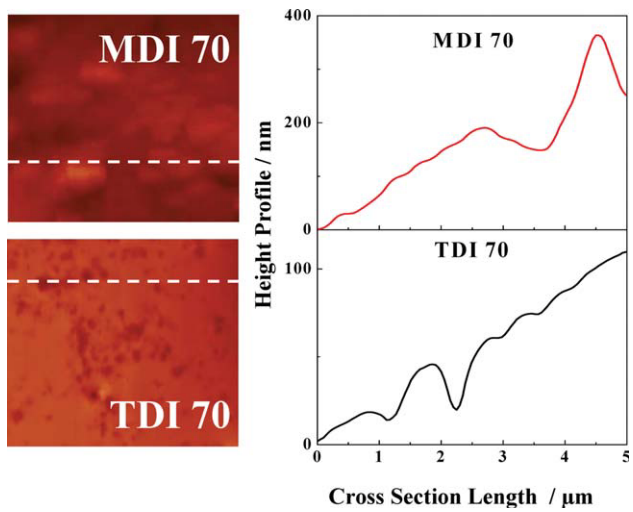

Figure 9 The height profile of the indicated aromatic PUs for higher HSC (right side figures). The profiles were obtained from the AFM topographs of the portion shown by dashed line in the left side of the figure. [Color figure can be viewed in the online issue, which is available at wileyonlinelibrary.com.]

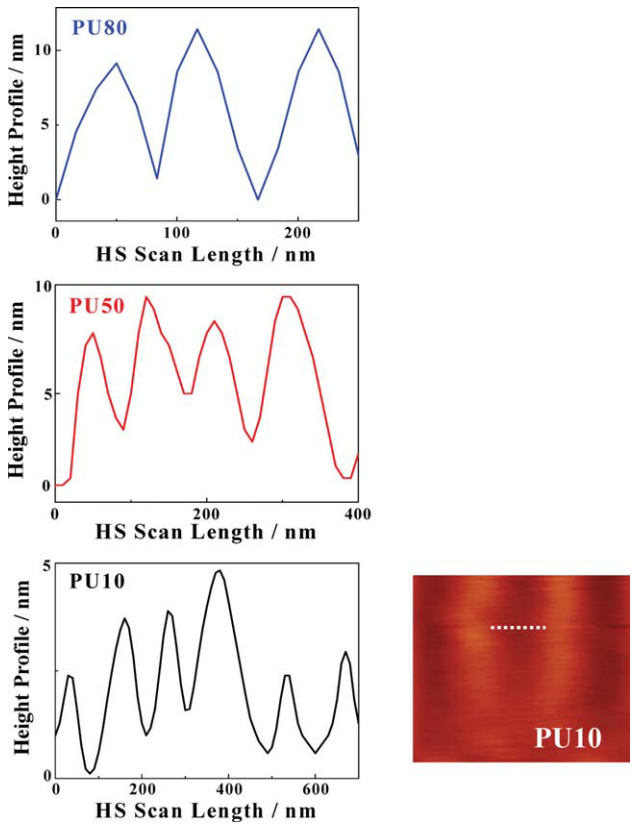

Figure 10 The height profiles for single domain of indicated aliphatic PUs (left side figures). The profile was obtained from the representative AFM topograph of the portion shown by dashed line in the right side of the figure. [Color figure can be viewed in the online issue, which is available at wileyonlinelibrary.com.]

same time, width of the individual domain decrease with increasing HSC. Interestingly, the micro-domain width is ~100 nm irrespective of the HSC of aliphatic PUs as calculated from the number of micro-domain and individual domain width. Micro-domain size is same for every HSC PU while the extent of self-assembly of those micro-domains leading to construct a domain considerably depends on HSC. In other words, three micro-domains can form a single domain for 80% HSC PU against the necessary six micro-domains to create a single domain for 10% HSC PU (Fig. 10). The greater interactions as a result of more number of urethane linkages, responsible for hydrogen bonding, for higher HSC samples limit the number of micro-domains to construct a single domain. On the other hand, more number micro-domains are required for self-assembly for lower HSC PUs as the hydrogen bonded interaction sites are less. Although the micro-domain size is same for every HSC PU but the ultimate domain size is different and depends on hard segment content.

To look inside a domain structure, XRD patterns of aliphatic and aromatic PUs with high HSC have been presented in Figure 11. Aliphatic PU80 shows a strong peak corresponding to *d*-spacing of 1.6 nm while aromatic PUs do not exhibit any such peak. The peak at low angle represents the ordered planar structure of polymer which is categorically absent in aromatic PUs. The planar structure arises from the periodic arrangement of hard segments which assemble together through hydrogen bonding to create a micro-domain, and further assembly of micro-domain gives rise to a domain structure observed in AFM images. Similarly, few domains auxiliary pile up again through hydrogen bonding to form a network structure observed in POM images. The self-assembly is evident in aliphatic PUs starting from nanometer dimension to micron size while lack of hydrogen bonding prohibits the formation of nano-structure due to bulky aromatic group in the backbone chain of aromatic PUs. Therefore, considerable self-assembly has not occurred in aromatic polyurethanes, and as a result, domain structure cannot form in TDI- and MDI- based PUs in contrast to HMDI- based aliphatic one.

Surface and bulk domain morphology

Figure 12(a) shows the scanning electron micrographs of aliphatic polyurethanes with increasing hard segment content. The micro-clusters, as observed in optical images, are also clear in the surface morphology with increasing HSC content. PU10 shows amorphous morphology against the hard fragmented zones noticed in PU80. The systematic growth of crystalline domains leads to smaller clusters. The amorphous nature of aromatic PUs has clearly been observed in Figure 12(b) even at high HSC. However, self-assembled stacking patterns leading to hard fragmented zone have been examined in crystalline

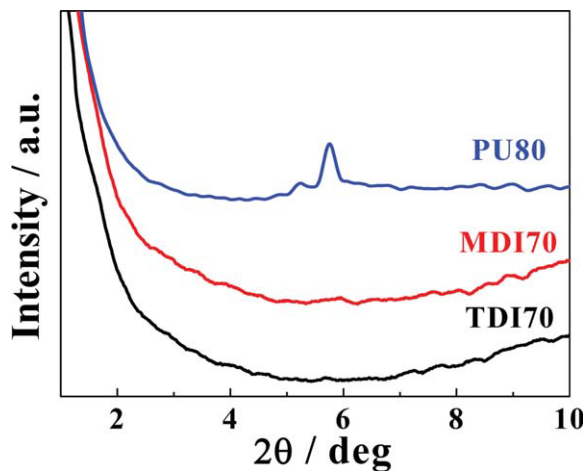

Figure 11 The X-ray diffraction patterns for indicated aliphatic and aromatic PUs of high HSC. The Y-axes have been shifted for the sake of clarity. The numbers after PU indicate the hard segment content in percentage. [Color figure can be viewed in the online issue, which is available at wileyonlinelibrary.com.]

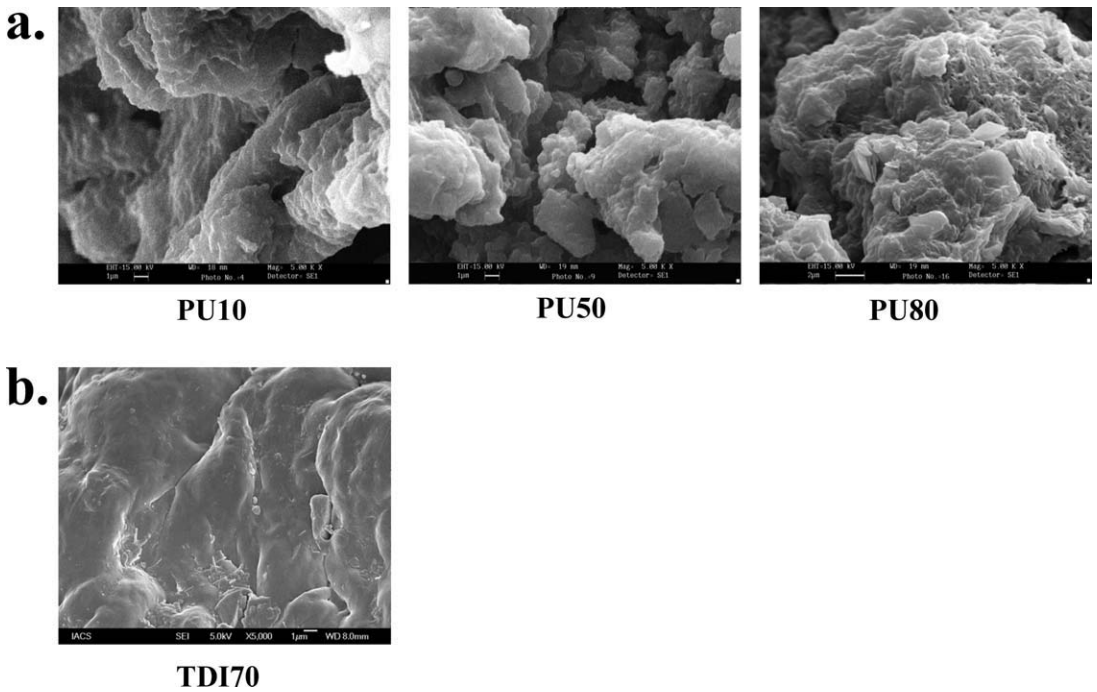

Figure 12 Scanning electron micrographs of polyurethanes with different hard segment content PU showing amorphous nature for low HSC content sample while crystalline clusters are evident for high HSC sample with a gradual change over from amorphous to crystalline morphology, (a) aliphatic and (b) aromatic polyurethane. [Color figure can be viewed in the online issue, which is available at wileyonlinelibrary.com.]

aliphatic PUs, while amorphous morphology is obvious for aromatic PUs as well as lower HSC aliphatic PUs.

Bright field TEM image of PU20 stained with 2 wt % phosphotungstic acid has been shown in Figure 13. The white patches indicate the crystalline zone and the dark black areas designate the amorphous zone. The phase contrast, as revealed in the micrograph, denotes the hard segment content present in polyurethane is due to deposition of heavy metal ions especially in the amorphous region. Comparatively less hard segments zones have been observed as the HSC content is less in PU20. However, smaller clusters have been detected in aliphatic PUs both in surface and bulk while aromatic PUs do not exhibit any such clusters.

Light microscopy

To understand the phase behavior of polymer with varying temperature, light transmittance has been conducted. The experimental setup for light transmittance has been shown in Scheme 1 where the specimen was kept under a heating program in hot stage and the intensity of the transmitted light was monitored by using a photodiode. Initially, the intensities of transmitted light decrease gradually with increasing temperature for every hard segment content aliphatic PU (Fig. 14). Further, the intensity starts increasing beyond certain temperature for respective PUs. The transition point is the homogenization temperature and is located on the onset of melting behavior, as evident from the DSC thermogrammes (Fig. 3). More light can transmit through the film when homogenization/melting occurs resulting up-turn of the intensity curves. The homogenization/melting occur at 90°C, 130°C, and 162°C for PU10, PU50, and PU80, respectively. In contrast, there is no change in intensity with temperature for aromatic TDI-based PU. The reason may lie on no-

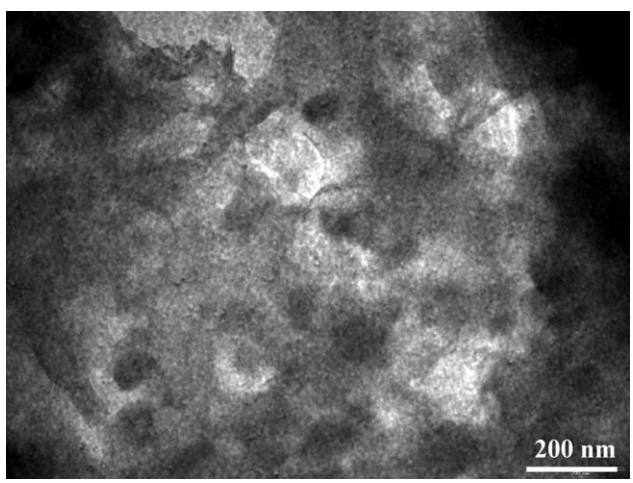

Figure 13 Bright field TEM image of PU20. The specimen was stained with PTA. [Color figure can be viewed in the online issue, which is available at wileyonlinelibrary.com.]

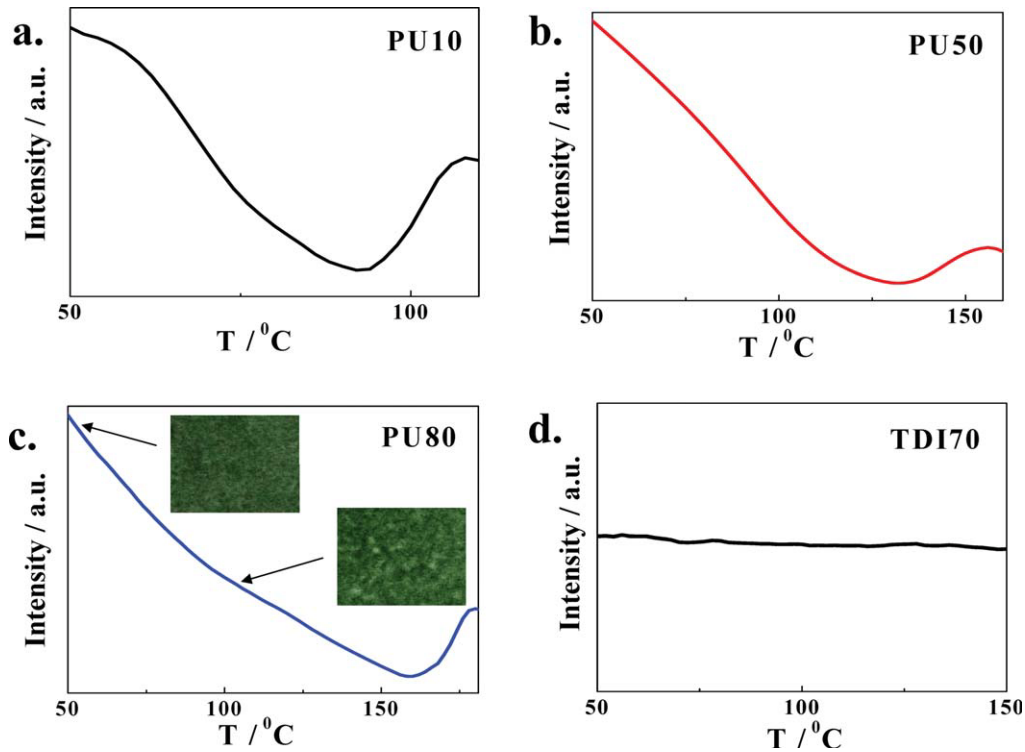

Figure 14 The intensity of the transmitted light as a function of temperature, a) PU10, b) PU50, c) PU80, and d) TDI70. The inset images for PU80 have taken at indicated temperature showing clustering at different temperature range. [Color figure can be viewed in the online issue, which is available at wileyonlinelibrary.com.]

phase separation of aromatic PU with increasing temperature, as evident from POM image as well (Fig. 2). The initial decrease of intensity for aliphatic PUs is presumably due to the phase separation which takes place with increasing temperature as a result of crystallization and subsequent segmentization. The phase separation is evident from the optical images taken at two different temperatures (inset images in PU80- where the effect is prominent) during the scanning of temperature in hot stage. At 50°C predominantly single phase was observed while two phase morphology was clear at 100°C. The segregation of phases cause the reduction in intensities of the scatter light with increasing temperature as a result of enhanced crystallization. Hence, light microscopy proves the phase separation of aliphatic PUs with varying temperature and hard segment content while aromatic PUs do not exhibit any phase separation irrespective of hard segment content.

CONCLUSIONS

Comparison of self-assembly behavior has been made of aliphatic and aromatic polyurethanes containing 10 to 80% hard segment content. DSC and XRD studies reveal that crystallinity increases with increasing HSC of aliphatic PUs while aromatic PUs are amorphous through out the entire range of HSC studied here. The melting temperature as well as heat of fusion increases with increasing HSC. Two phase morphology has been seen in aliphatic PUs and mostly single phase has been observed in aromatic PUs. AFM topographs exhibit banded domains for aliphatic PUs and the dimension of the domain gradually decreases with increasing HSC. Further, scanning of individual domain indicates the self-assembly of few micro-domains of size ~100 nm irrespective of HSC content. On the contrary, aromatic PUs show nanoscopic band which could not grow up to domain structure. The self-assembled structure formation in aliphatic polyurethane has

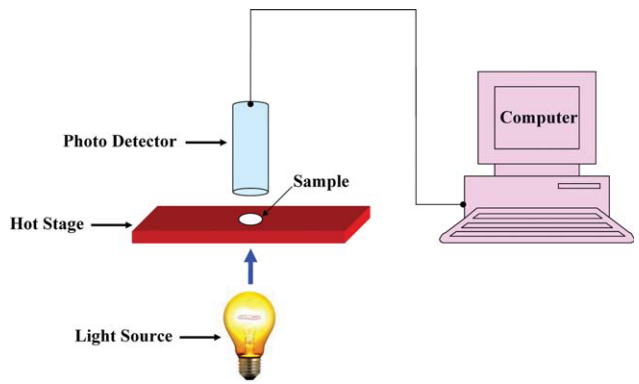

Scheme 1 The schematic view for the light transmittance experiment.

been demonstrated through POM, AFM, and SEM. TEM image of PU20 shows the distribution of crystalline domains in the soft segment matrix. XRD reveals the stacked patterns of hard segments of aliphatic PUs as evident from the peak corresponding to interplanar *d*-spacing of 1.6 nm. Step by step self-assembly occurs via intermolecular hydrogen bonding in the hard segment zones. Separation of two phases for aliphatic polyurethanes has been observed by light microscopy experiment in contrast to aromatic polyurethanes.

The authors acknowledge the kind support of Prof. Gajendra Singh and Dr. Madhu Yashpal for TEM observation as well as Dr. D.K. Avasthi and Mr. Pawan K. Kulriya of IUAC, New Delhi for XRD measurements.

References

1. Thomson, T. Polyurethanes as Specialty Chemicals: Principles and Applications; CRC Press: Boca Raton, 2005.
2. Szycher, M. Szycher's Handbook of Polyurethanes; CRC Press: Boca Raton, 1999.
3. Wirpsza, Z. Polyurethanes: Chemistry, Technology and Application; Harwood Publs.: New York, 1993.
4. Hepburn, C. Polyurethane Elastomers, 2nd ed.; Elsevier Applied Science Publ.: London, 1991.
5. Peppas, N. A.; Langer, R. Science 1994, 263, 1715.
6. Koevoets, R. A.; Versteegen, R. M.; Kooijman, H.; Spek, A. L.; Sijbesma, R. P.; Meijer, E. W. J Am Chem Soc 2005, 127, 2999.
7. Lendlein, A.; Langer, R. Science 2002, 296, 1673.
8. Banerjee, S.; Mishra, A.; Singh, M. M.; Maiti, P. J Nanosci Nanotechnol, to appear.
9. Langer, R.; Tirrell, D. A. Nature 2004, 428, 487.
10. Lendlein, A.; Jiang, H.; Junger, O.; Langer, R. Nature 2005, 434, 879.
11. Wisse, E.; Spiering, A. J. H.; vanLeeuwen, E. N. M.; Renken, R. A. E.; Dankers, P. Y. W.; Brouwer, L. A.; vanLuyn, M. J. A.; Harmsen, M. C.; Sommerdijk, N. A. J. M.; Meijer, E. J. Biomacromolecules 2006, 7, 3385.
12. Boretos, J. W.; Pierce, W. S. Science 1967, 158, 1481.
13. Lee, B. S.; Chun, B. C.; Chung, Y. C.; Sul, K. I.; Cho, J. W. Macromolecules 2001, 34, 6431.
14. Yilgor, E.; Yilgor, I.; Yurtsever, E. Polymer 2002, 43, 6551.
15. Yilgor, E.; Yurtsever, E.; Yilgor, I. Polymer 2002, 43, 6561.
16. Shimura, Y.; Chen, D. Macromolecules 1993, 26, 5004.
17. Boufi, S.; Belgacem, M. N.; Quillerou, J.; Gandini, A. Macromolecules 1993, 26, 6706.
18. Wang, C. B.; Cooper, S. L. Macromolecules 1983, 16, 775.
19. Nitzsche, S. A.; Hsu, S. L.; Hammond, P. T.; Rubner, M. F. Macromolecules 1992, 25, 2391.
20. Zhang, J.; Hu, C. P. Euro Polym J 44: 3708 2008.
21. Kojio, K.; Nakashima, S.; Furukawa, M. Polymer 2007, 48, 997.
22. Maiti, P.; Radhakrishnan, D.; Aruna, P.; Ghosh, G. Macromol Symp 2006, 241, 51.
23. Miller, J. A.; Lin, S. B.; Hwang, K. K. S.; Wu, K. S.; Gibson, P. E.; Cooper, S. L. Macromolecules 1985, 18, 32.
24. Teo, L. S.; Chen, C. Y.; Kuo, J. F. Macromolecules 1997, 30, 1793.
25. Velankar, S.; Cooper, S. L. Macromolecules 1998, 31, 9181.
26. Velankar, S.; Cooper, S. L. Macromolecules 2000, 33, 395.
27. Williams, S. R.; Wang, W.; Winey, K. I.; Long, T. E. Macromolecules 2008, 41, 9072.
28. Li, Y.; Ren, Z.; Zhao, M.; Yang, H.; Chu, B. Macromolecules 1993, 26, 612.
29. Lee, J. B.; Kato, T.; Yoshida, T.; Uryu, T. Macromolecules 1993, 26, 4989.
30. Nair, B. R.; Osbourne, A. R.; Hammond, P. T. Macromolecules 1998, 31, 8749.
31. Jeong, H. M.; Kim, B. K.; Choi, Y. J. Polymer 2000, 41, 1849.
32. Versteegen, R. M.; Kleppinger, R.; Sijbesma, R. P.; Meijer, E. W. Macromolecules 2006, 39, 772.
33. Hernandez, R.; Weksler, J.; Padsalgikar, A.; Choi, T.; Angelo, E.; Lin, J. S.; Xu, L. C.; Siedlecki, C. A.; Runt, J. Macromolecules 2008, 41, 9767.
34. Klinedinst, D. B.; Yilgor, E.; Yilgor, I.; Beyer, F. L.; Wilkes, G. L. Polymer 2005, 46, 10191.
35. McLean, R. S.; Sauer, B. B. Macromolecules 1997, 30, 8314.
36. Sheth, J. P.; Wilkes, G. L.; Fornof, A. R.; Long, T. E.; Yilgor, I. Macromolecules 2005, 38, 5681.
37. Sheth, J. P.; Klinedinst, D. B.; Pechar, T. W.; Wilkes, G. L.; Yilgor, E.; Yilgor, I. Macromolecules 2005, 38, 10074.
38. Mishra, A.; Aswal, V. K.; Maiti, P. J Phys Chem B 2010, 114, 5292.